VALIDATION OF CFD CODES FOR THE HELICOPTER WAKE IN GROUND EFFECT

Masahiko Sugiura, JAXA, Tokyo, Japan
Yasutada Tanabe, JAXA, Tokyo, Japan
Hideaki Sugawara, Ryoyu Systems, Aichi, Japan
George N. Barakos, the University of Glasgow, Glasgow, United Kingdom
Naoki Matayoshi, JAXA, Tokyo, Japan
Hirokazu Ishii, JAXA, Tokyo, Japan

Abstract

When a helicopter takes off, lands, or makes hovering or taxiing flights in ground effect, its downwash interferes with the ground. Encounters with such highly turbulent helicopter wakes have been blamed for two fixed-wing aircraft crashes in the United Kingdom. Additional incidents including tents blown away are reported in Japan. Due to these accidents, the Japan Aerospace Exploration Agency (JAXA) and the University of Glasgow (UoG) are investigating the helicopter wake structure in ground effect, especially during taxiing, by means of computational fluid dynamics (CFD). In this study, CFD codes of UoG and JAXA are validated through comparing numerical results of each party and flight experiment data. As a result, it is found that the CFD codes show qualitatively the same results each other and they are also close to the experiment.

1. INTRODUCTION

Minimum separation distances between aircraft are enforced to avoid wake turbulence encounters. Using the ICAO classification system, helicopters are defined as light aircraft, since they are relatively small compared to commercial fixed-wing airplanes. Thus, the wake turbulence separation for a helicopter is frequently set at 3.0 NM. However, this separation is not practical when helicopter size is considered, and there is an additional guideline recommending at least three rotor radii of separation (FAA, CAA). A helicopter itself may not be severely affected by the blade tip vortex of a fixed-wing aircraft, since the effects of gusts are milder on rotor blades [1]; however, a helicopter's wake itself is strong and complex, and it may have adverse effects on fixed-wing aircraft operating nearby, as well as, on objects and people on the ground. Two fixed-wing aircraft accidents occurred in the United Kingdom allegedly due to encountering the wakes of helicopters while landing at airports in the 1990s [2]. One more incident recently happened in Japan, in which the wakes of a helicopter blew away three tents at a camp site [3]. Despite the serious nature of these accidents, wake turbulence separation distances and operational guidelines for helicopters have still not been determined. This is mainly due to lack of in-depth understanding of the helicopter wakes physics and of scientific evidence that could be used to reduce the hazard of wake turbulence encounter. In this study, numerical analysis and validation of CFD tools were conducted aiming to support decisions on wake turbulence separation minima for helicopters in airports, and to establish operational guidelines.

In previous studies, helicopter wakes were investigated using LIDAR, alongside fixed-wing aircraft studies, mainly in the United States of America [4]. The initial circulation of the wake and the maximum wake detectability range were measured for many types of helicopters. Larger helicopters sustained wakes longer than smaller helicopters.

Recently, piloted simulation of a light aircraft encountering a helicopter wake was conducted by the Universities of Glasgow (UoG) and Liverpool to assess the validity of the three rotor diameter guideline [5]. The simulation indicated that the wake effects were reduced to insignificant levels after the wake decayed to 50% of its full strength. In that paper, numerical methods such as the prescribed wake model, free wake model, and computational fluid dynamics (CFD) with actuator disc theory were also compared with the experiment. The computational accuracy of CFD with actuator disc theory was the highest among these numerical methods, and this method has been applied in flight simulators.

On the other hand, the Japan Aerospace Exploration Agency (JAXA) has long been developing the rFlow3D CFD code for rotorcraft [6] and investigated the helicopter wake in ground effect [7, 8]. In Ref. [7], the velocity profiles of the isolated rotor

downwash in ground effect were modelled applying Euler's equations and a wall jet model in the near and far wakes, respectively. The computational predictions correlated well with the experimental results when the distance from the rotor hub was less than a rotor diameter, but agreement worsened as separation increased. In Ref. [8], the helicopter wake was measured in flight tests and simulated by computational fluid dynamics (CFD) simultaneously. The characteristic wake structure variations with taxiing speed were clearly observed in the CFD results and were supported indirectly by the flight experiment results. The following were observed in the numerical analyses: 1) when the taxiing speed was higher than 30 kts, the helicopter wake developed horseshoe vortices, similar to those of a fixed-wing aircraft; 2) as the taxiing speed decreased, the horseshoe vortices spread horizontally, which is also similar to the behaviour of a fixed-wing aircraft blade tip vortex in ground effect; 3) there was a possibility of brownout, although strong vortices near the rear of the fuselage did not exist when the taxiing speed was lower than 20 kts. From flight experiments, the following results were obtained: 1) the merging of the helicopter wake into a single vortex was visualized by smoke at a TAS of 30 kts; 2) the wake descending speed decreased due to ground effects as the helicopter altitude decreased; 3) the wake endurance time increased as the TAS increased; 4) vortex characteristic wind speed was captured by an ultrasonic anemometer at TASs of 30 kts and 40 kts.

In this study, CFD codes of UoG and JAXA are compared using numerical results of each party and flight experiment data.

2. NUMERICAL METHODS

Each party has been developing their numerical methods independently though, there are similarities in the underlying CFD methods. In this section, the employed numerical methods are elaborated.

2.1. UoG

A chimera grid is used for the numerical simulations by UoG. The chimera meshing method has several advantages. For example, the grid is simpler to move, in particular when a complex geometry is involved such as the present fuselage shown in Fig. 1. Two sub-grids are used in the current study: one is the background grid, which is Cartesian and refined near its center in the spanwise direction, and around the helicopter, in the streamwise direction, as shown in Fig. 2. In that figure, a grid of 16R width and 75R length downstream the helicopter, is shown, along with a detailed view in the helicopter area. A second background has been designed for low advance ratio cases, at which the wake and downwash generated by the rotor in ground effect is larger. As a consequence, the grid width was increased to 20R, and its length in the streamwise direction was shortened to 50R, as shown in Fig. 3. This was needed to keep the number of computational cells reasonable.

Table 1 shows the employed grid densities. The second grid is finer and contains the fuselage geometry. The outer boundary of this domain has a cylindrical shape in the present case. This sub-grid is embedded in the background grid and allows for modifying in an easy and rapid way the position of the helicopter, e. g. the height over the ground.

An ONERA 7AD1 blade [8] was used for the main rotor and MBB-S102E for the tail rotor in the analysis; their specifications are summarized in Table 2. In this study, the ONERA 7AD1 blade was expanded in the spanwise direction to match a fuselage size. On UoG side, the main and tail rotors are treated as actuator disks. The fuselage geometry is similar (but not an exact representation) of the H145 (EC145, BK117 C-2, Fig. 5) used for tests by JAXA.

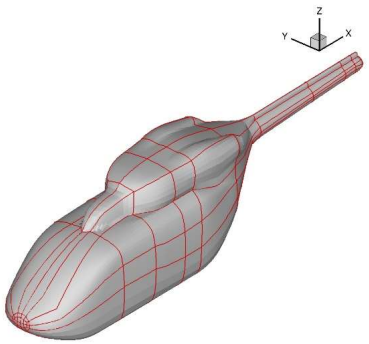

Fig. 1. View of the approximate helicopter fuselage used for UoG's simulations.

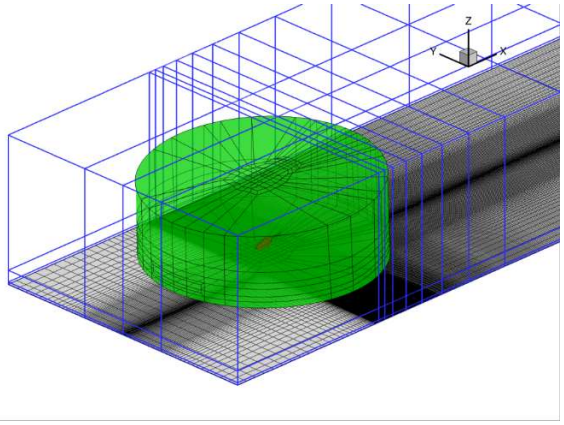

Fig. 2. H145 IGE chimera domain, 30-ft test case. This mesh is used for computations at high advance ratio.

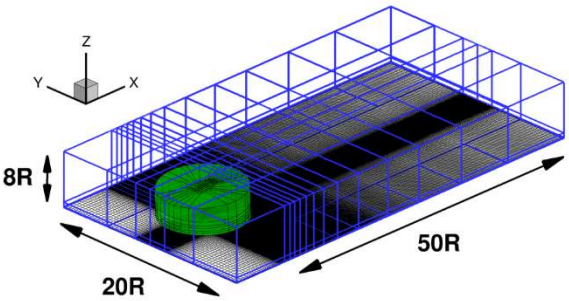

Fig. 3. H145 IGE wider chimera domain, 30-ft test case, designed for lower advance ratio.

Table 1: Number of cells used for numerical computations of UoG.

Long domain	Large domain
32,191,730	33,314,296

Table 2: Approximate rotor system.

	Main rotor	Tail rotor
Number of blades	4	2
Rotor radius	5.5 m	0.978 m
Chord length	0.41 m	0.22 m
Aerofoil	ONERA 7AD1: ONERA 213 (from root to 0.7*R*) ONERA 209 (from 0.9R to tip)	MBB-S102E

2.2. JAXA

The base CFD code of JAXA was the structured overlapping grid flow solver, rFlow3D, which has been systematically developed for rotorcraft applications [5]. The rFlow3D solver is a highly versatile CFD code that can numerically simulate flows around rotorcraft with a wide range of Reynolds and Mach numbers and can perform rotor trim analysis with elastic blade deformations. The previous study showed that the isolated rotor results obtained by the N-S equations yielded results closer to the experiment than those obtained using Euler equations [7]. Thus, the N-S equations were applied in this study. An unstructured grid flow-solver TAS-code developed at Tohoku University in Japan was combined with rFlow3D to simulate the flow around a fuselage, which has a complex geometry. Figure 4 shows the computational grids, which contain approximately twenty million points. The model helicopter used for JAXA's simulation is also shown in Fig. 5. On the JAXA side, the main rotor blade grids are rotated with the moving overlapping grids, but the tail rotor is not taken into account in this study. Nevertheless, the empennage is modelled more precisely, compared to UoG with horizontal stabilizer, fin and end-plates included.

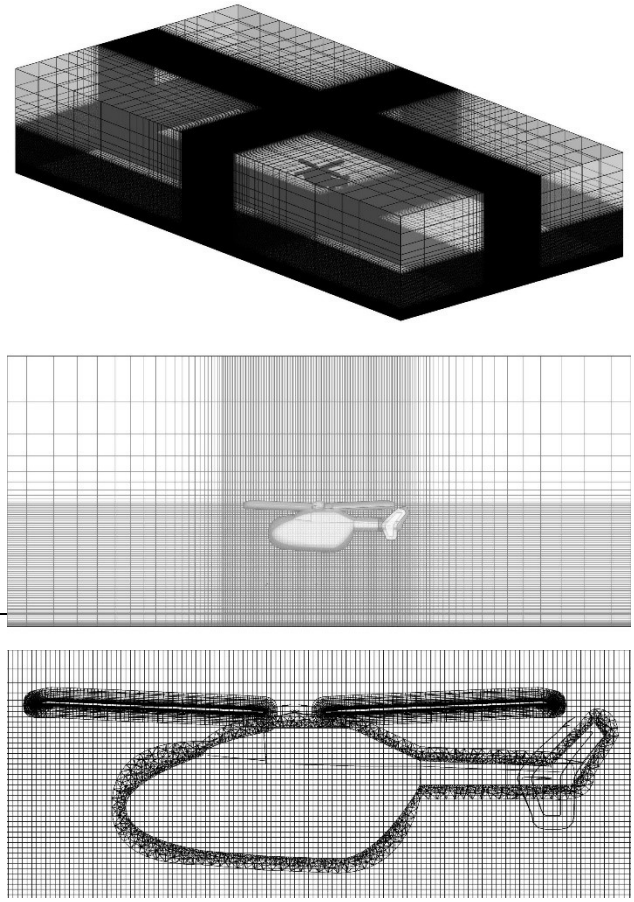

Fig. 4. JAXA computational grids (R: radius of the rotor).

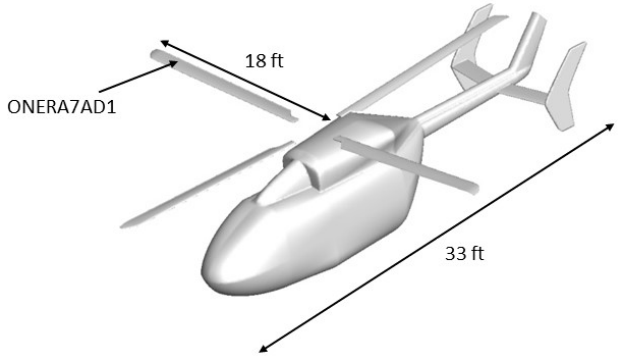

Fig. 5. Model helicopter used for JAXA's simulation.

3. NUMERICAL CONDITIONS

Flight tests of measuring wakes of JAXA's research helicopter's (Fig. 6) were conducted at the end of October 2014 at the Taiki Aerospace Research Field (coordinates: 42.498795, 143.433397) of the Hokkaido Prefecture in Japan. The exact dimensions of H145 are given in Fig. 7. The wakes were measured using LIDAR and ultrasonic anemometers (Fig. 8). The employed LIDAR was of the all-fibre, pulsed, coherent Doppler type, with velocity resolution approx. 3ft/s and measurement rate of 10 Hz. Ultrasonic anemometers were used at a measurement height of 8.2ft (2.5 m) and sampled at a rate of 10 Hz. The specifications of the LIDAR and the ultrasonic anemometers are summarized in Table 3. While conducting these measurements, smoke visualization of the helicopter wake (Fig. 9) was also conducted to confirm the numerical results. A fog generator (HIT800C, Kawada Industries, Inc., Japan) was utilized. Smoke was generated by burning the fog-generating liquid that is nearly identical to paraffin oil.

Figures 10 and 11 summarise the setup and the arrangements of the tests. Using maps and photographs in the public domain, the scene of the tests was re-created. In this experiment, flight tests were conducted 42 times over 3 days. Figure 12 shows the test points of the campaign. The target forward speeds of the helicopter were 0 kts, 5 kts, 10 kts, 15 kts, 20 kts, 30 kts, and 40 kts. The flight altitude expressed as rotor head altitude varied from around 20 ft to70 ft. The red circles correspond to cases simulated using CFD. The exact conditions of the CFD tests are given in Table 4. And Table 5 summarises the flow conditions used for computations. The reference length used in the Reynolds number calculation is the non-dimensionalised chord c = 1 of the helicopter rotor blade as follows;

$$Re = \frac{\rho V_0 c}{\nu} = \frac{1.225\, V_o}{1.7864 \,.\, 10^{-5}} \quad (1)$$

Table 6 presents the approximate rotor systems used in this study. The rotor is approximated as a disk with a tail rotor on UoG side. The rotor power is then;

$$P = \frac{1}{8}\rho V_{\text{tip}}^3 N_b c R C_D + \frac{T^{3/2}}{\sqrt{2\rho A}} = 98957\ Nm/s \quad (2)$$

where ρ is the air density, V_{tip} is the blade tip velocity, N_b is the number of blades, c is the blade chord, R is the rotor radius, C_D is the drag coefficient, T is the thrust, A is the area of the rotor ($A = \pi R^2$). Then, the power can be related to torque using,

$$P = \vec{Q}.\vec{\Omega} \quad (3)$$

which gives Q = 2465 kg.m^2.s^{-2}.

The tail rotor was located at a distance of 6.55 m from the main rotor rotation axis, so:

$$T_{\text{tail}} = 2465 \text{ x } 6.55 = 16146\ N \quad (4)$$

$$C_T = \frac{T}{0.5\rho_\infty V_{\text{tip}}^2 A} = 0.0057 \quad (5)$$

Fig. 6. JAXA's research helicopter: H145 (EC145, BK117 C-2).

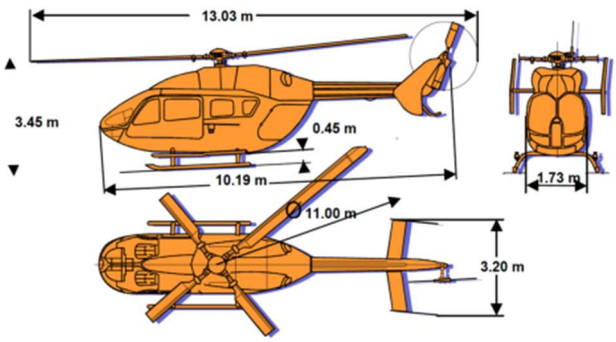

Fig. 7. H145 (EC145, BK117 C-2) dimensions from Ref. [9].

Fig. 8. Equipment used to measure helicopter wake.

Table 3: Specifications of measurement equipment.

LIDAR #1: WINDCUBE200S, LEOSPHERE, France	
Measurement Data	Wind Speed in the Line of Sight, Velocity Width, SN Ratio, Doppler Spectrum
Measurement Range	Approx. 0.6~1.2 mi
Measurement Rate	10 Hz
Range Resolution	17 ft
Velocity Resolution	Approx. 3 ft/s
Scanning Methods	Fixed Line of Sight, Constant Elevation Angle, Constant Azimuth Angle

LIDAR #2: LR-09FLIII, Mitsubishi Electric, Japan	
Measurement Data	Wind Speed in the Line of Sight, Velocity Width, SN Ratio, Doppler Spectrum
Measurement Range	550 yards
Measurement Rate	4 Hz
Range Resolution	33~125 ft
Velocity Resolution	3 ft/s
Scanning Method	Fixed Line of Sight, Constant Elevation Angle, Constant Azimuth Angle

CYG-81000, R. M. Young Company, USA	
Measurement Data	Three Axes of Wind Speed
Measurement Rate	10 Hz

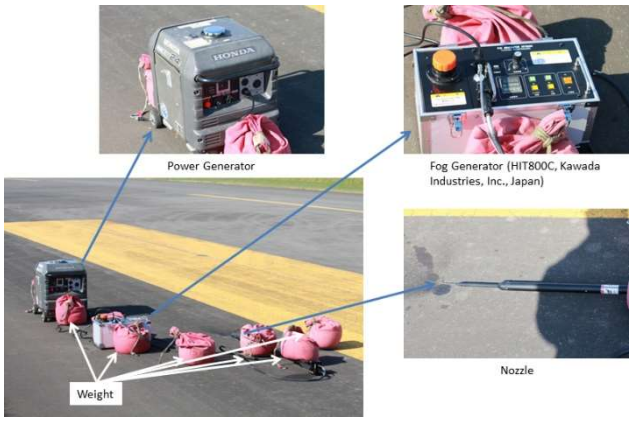

Fig. 9. Smoke visualization equipment.

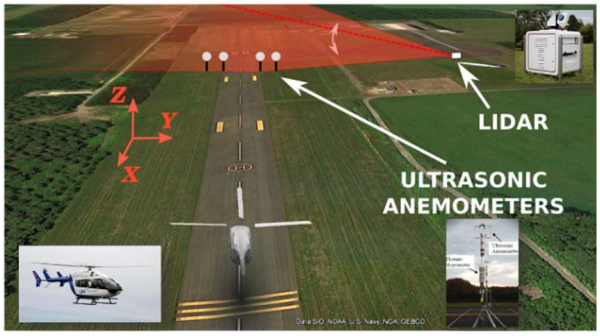

Fig. 10. Field view of the experimental setup.

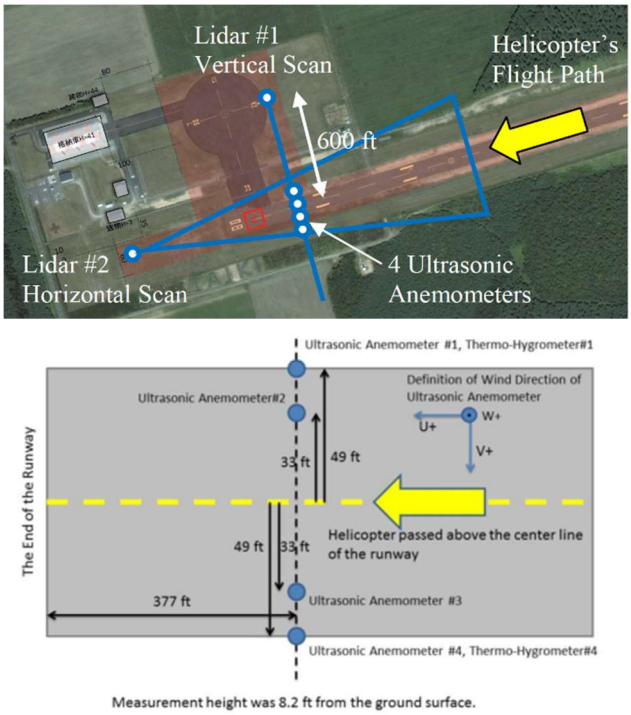

Fig. 11. Helicopter wake measurement pattern by LIDAR and ultrasonic anemometer (LIDAR #2 for horizontal measurements was not used) (top) and configurations of ultrasonic anemometers and thermo-hygrometers on the runway (bottom) from Ref. [8].

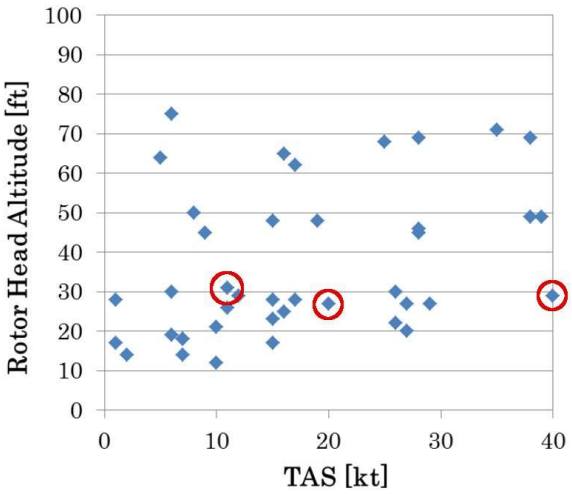

Fig. 12 Experimental flight conditions from Ref. [8]. Circled test-cases are retained for the simulations.

Table 4: Flight conditions.

Taxiing Speed, kt	0, 10, 20, 40
Rotor Head Altitude, m	9.1
Trim Condition, kg	3,550 (Maximum Takeoff Weight)
Rotor Revolutions, rpm	383.36

Table 5: Simulation physical parameters of the flow.

V_∞, kt	10	20	40
V_∞, m/s	5.14	10.29	20.58
M_∞	0.0151	0.0302	0.0605
Re	352,773	705,546	1,411,093
μ_{main}	0.0233	0.0466	0.0931
μ_{tail}	0.0231	0.0463	0.0926

Table 6: Simulation physical parameters of the rotors (main rotor chord as reference length), all figures are approximate.

	Main rotor	Tail rotor
Number of blades	4	2
Rotor radius, m	5.5	0.978
Rotor radius (non dim.)	13.415	2.385
Chord length, m	0.41	0.22
Chord length (non dim.)	1.0	0.537
Solidity	0.095	0.1432
Cut out (diameter), m	1.45 (13% of rot. diam.)	0.45 (23% of rot. diam.)
RPM	383.36	2169.3
ω, rad/s	40.1	227.2
V_{tip}, m/s	220.8	222.2
M_{tip}, m/s	0.649	0.653

4. NUMERICAL RESULTS

Steady-state computations are carried for the case where the rotor is located 30 ft above the ground, at free-stream velocities of 10, 20 and 40 kts. Figure 13 shows the spatial extend of the wake captured by the CFD of UoG. When the taxiing speed is 10 or 20kts, we can see a bow shock-like concentration of vortices in front of the fuselage. On the other hand, as the taxiing speed increases to 40kts, the two vortices merge and the structure resembles more the vortex pair behind a fixed-wing aircraft. The dramatic change of the lateral expansion with the aircraft speed can also be seen.

Figure 14 shows similar figure from the JAXA CFD tools. The wake structure is coloured according to the horizontal velocity normalized by the speed of sound. When the taxiing speed is 10kts, a bow shock-like concentration of vortices is not as clear as in the UoG results, but the wake structures at 20kts are very similar between the two CFD codes. In addition, the horseshoe vortices are clearly observable at 40kts, too. Bird's eye view of Fig. 13 is also shown in Fig. 15.

Sectional vorticity distributions along the body axis at the taxiing speed of 40kts are compared in Fig. 16. From this figure, we can see that both sets of results clearly capture a pair of vortices. These numerical results are in good agreement with the flight experiments, where the phenomenon was clearly visualized by smoke as shown in Fig. 17.

Figure 18 shows flow details of UoG at the mid-plane of the domain. At the taxiing speeds of 10kts and 20kts, there are recirculation areas in front of the aircraft. And the characteristic flow is downwash regions at front and rear sides of the main rotor and downwash at the center. At 40kts, upwash in front of the aircraft and downwash at the rear becomes strongly apparent.

JAXA results are also shown in Fig. 19. The vertical velocity is contoured using the same scale as for UoG. The JAXA results are basically the same as UoG (Fig. 18), but there are some differences. When the taxiing speed is 10kts, upwash in front of the aircraft is stronger than for UoG and the area of upwash does not spread from the center of the main rotor backward as Fig. 18. This difference is supposed to be related to the differences in the employed analysis methods. UoG employs actuator disk for the main and tail rotors. On the other hand, JAXA simulates the main rotor by moving overlapping grids, but neglects the tail rotor's effect. Instead, the geometry of the empennage is modelled more precisely than UoG. An additional difference is that UoG uses a mirror condition for the ground while the computations of JAXA model ground as a solid surface. Thus, the region in front of the tail rotor is supposed to be simulated more accurately in JAXA CFD. At a taxiing speed of 20kts, the upwash in front of the aircraft is stronger than for UoG. And the downwash in the rear side of the aircraft at 40kts is not as strong as UoG's.

Figure 20 shows the corresponding velocity at the y-plane of the domain. Recirculation in front of the aircraft is confirmed as shown in Fig. 18, and the height of the wake increases as the taxiing speed increases.

In an attempt to compare with the LIDAR data for the wake, UoG used the setup shown in Fig. 21. The figure shows the extent of the computational domain and the location of the LIDAR system. Using this information, the data from the CFD were extracted on the scan-plane of the LIDAR and processed. As shown in Fig. 22, the wind speed in the line of sight from the LIDAR origin is plotted for several time instances (between 4 and 12 seconds) past the passage of the helicopter. The footprint of the tip vortex can be seen as a rapid change from blue to red colour. Following the red dashed line on the LIDAR data plot in Fig. 22, a similar change is seen as the line crosses the wake of the helicopter. At first low spectrum intensity in the LIDAR readings is seen followed by a rapid change as the wake crosses the scan line of the LIDAR. After the helicopter passes, the wake decays and slowly low spectrum intensity is seen. At the time of the writing, the raw LIDAR data was not available for further processing so that the qualitative comparison of Fig. 22 can become

quantitative by reconstructing from CFD the same information as the LIDAR was able to measure. This approach was applied in an earlier study reported in Ref. [10].

Figure 23 shows the time history of the wind speed in JAXA's CFD at the position of ultrasonic anemometer #1 (Fig. 11) with the experimental data. As the taxiing speed increases, the measurable time of the wind speed decreases, since the CFD computational region is constant despite the taxiing speed increase. Overall, the peak values of V and W in CFD are close to the experiment. When the taxiing speed was 40 kts, it was difficult to capture the time history of wind speed related to the vortex structure since the measurable time in CFD was rather short. However, the wind speed in CFD agrees well with the experiment in several seconds.

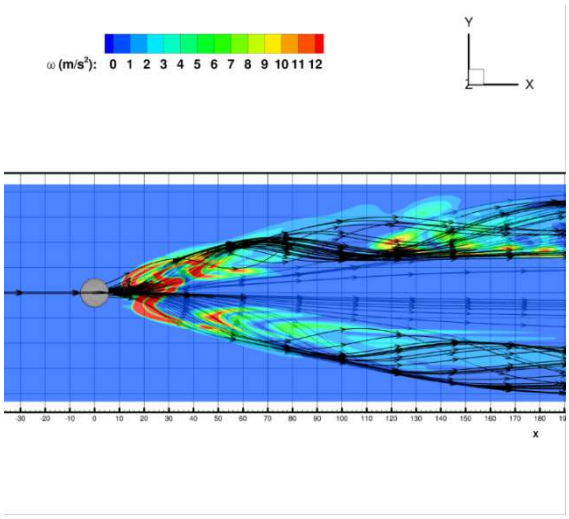

40kt

Fig. 13. Slice of vorticity magnitude at z = 1.5 m, along with streamline (UoG).

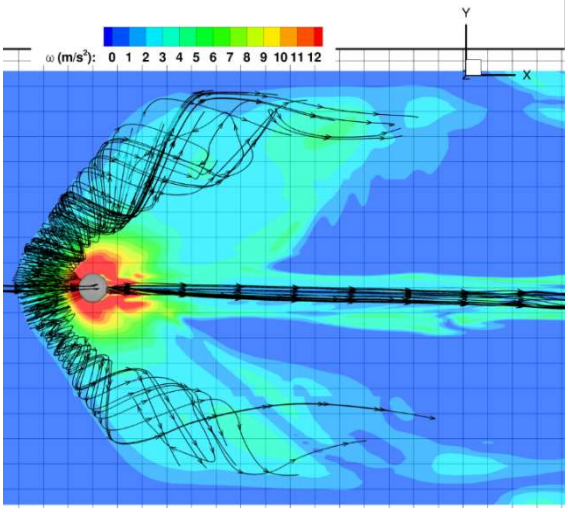

10kt

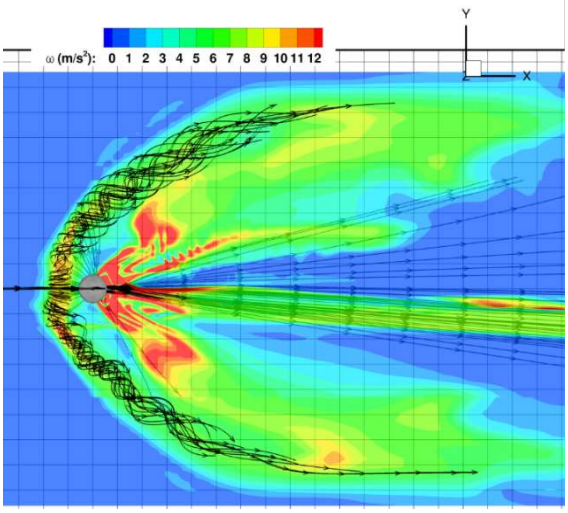

20kt

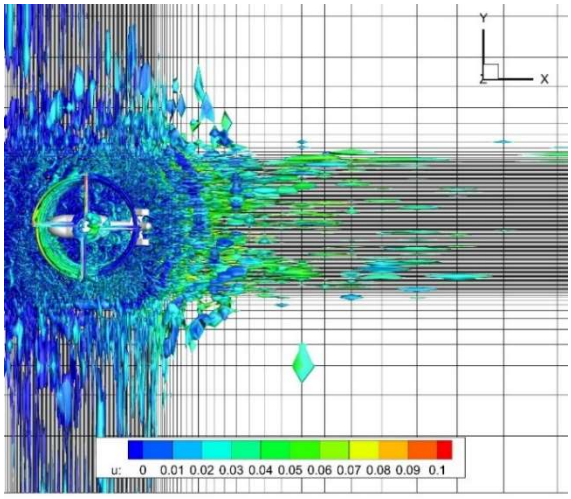

10kt

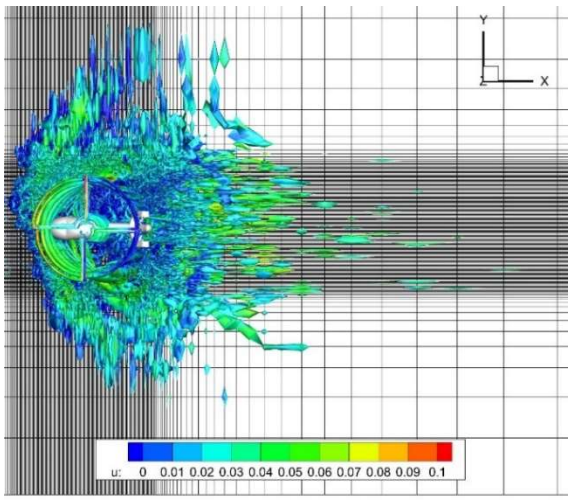

20kt

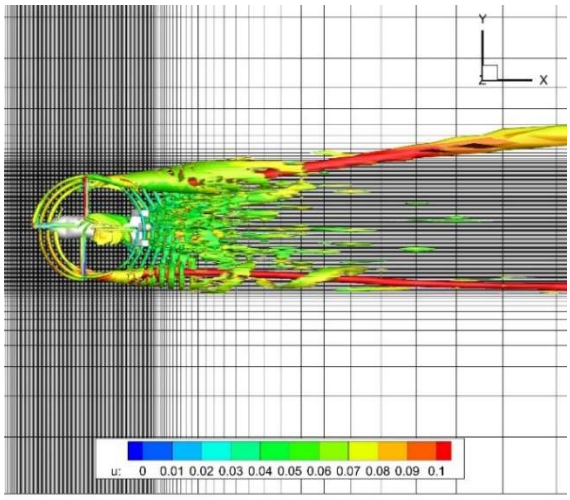

40kt

Fig. 14. Wake structure variation by taxiing speed (JAXA)

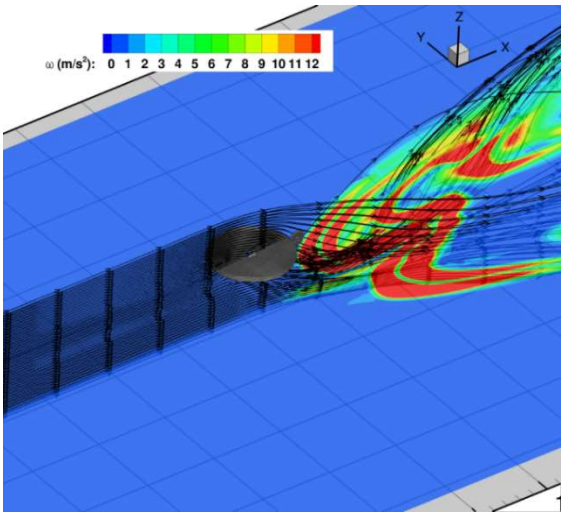

40kt

Fig. 15. Vorticity magnitude field overview on xy plane at z = 1.5 m, along with streamlines (UoG).

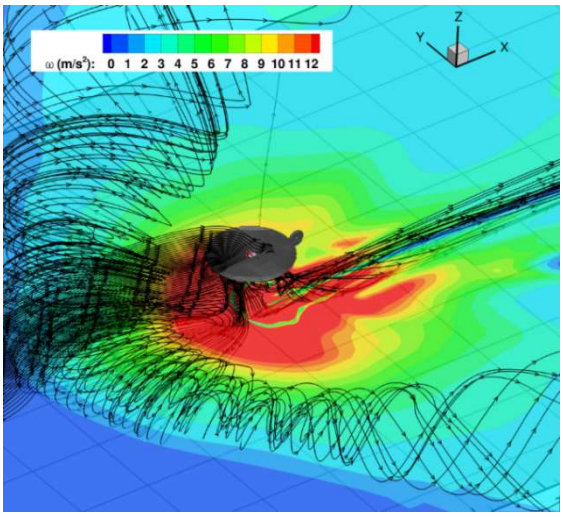

10kt

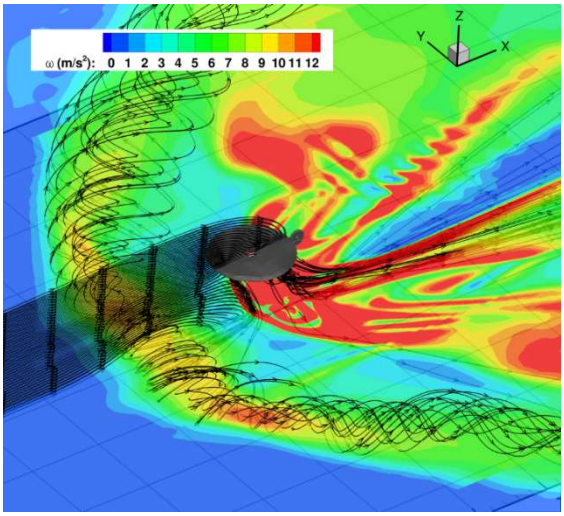

20kt

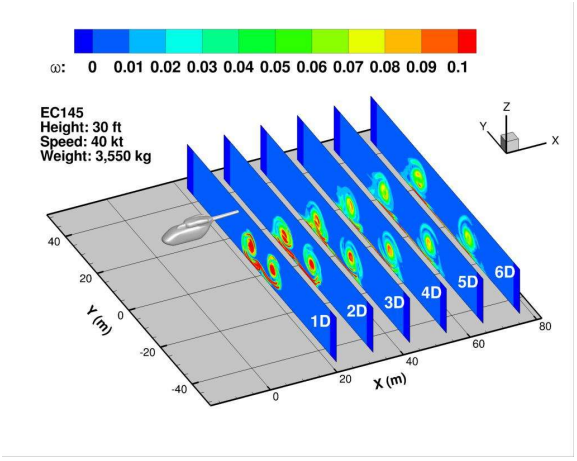

UoG

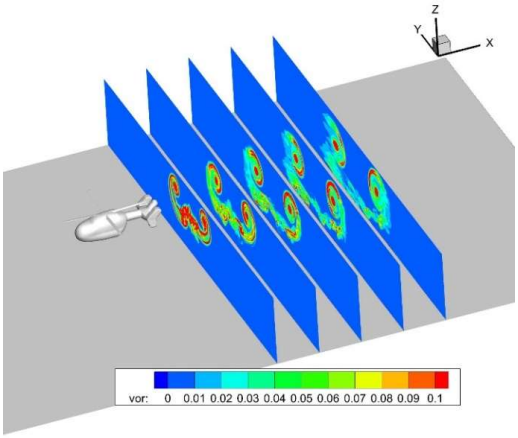

JAXA

Fig. 16. Sectional non-dimensional vorticity distributions along body axis at the taxiing speed of 40kts (D: diameter of rotor; vorticity is normalized by sonic speed and unit length).

Fig. 17. Visualization of helicopter wake by smoke.

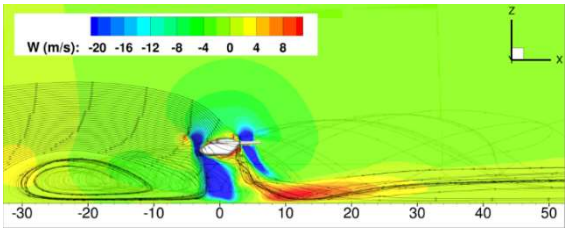

10kt

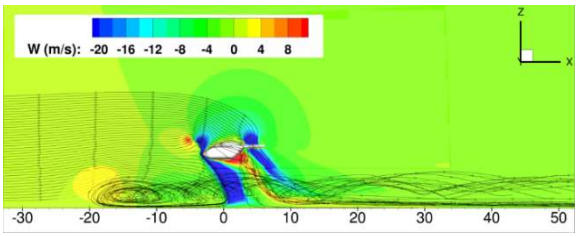

20kt

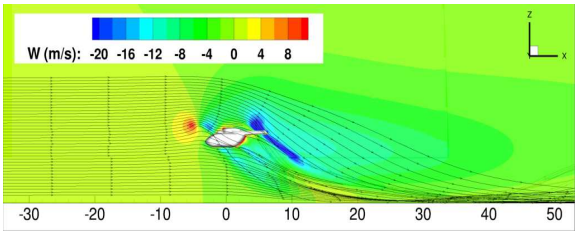

40kt

Fig. 18. Vertical velocity at the plane y = 0, along with streamlines (UoG).

10kt

20kt

40kt

Fig. 19. Vertical velocity at the plane y = 0 (JAXA).

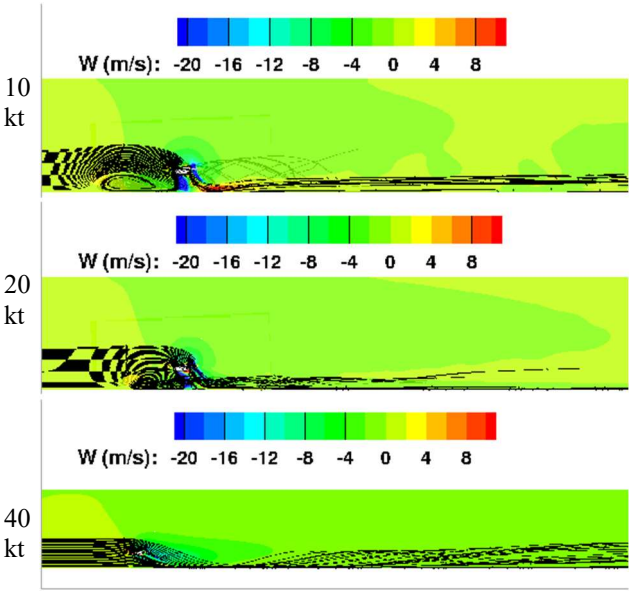

Fig. 20 Slice of vertical velocity at y = 0, along with streamlines.

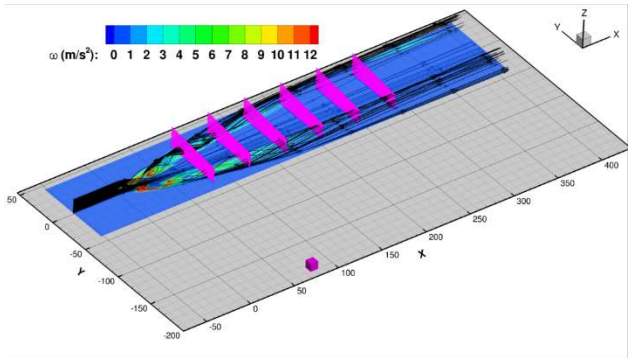

Fig. 21 Lidar location with respect to the CFD domain (UoG).

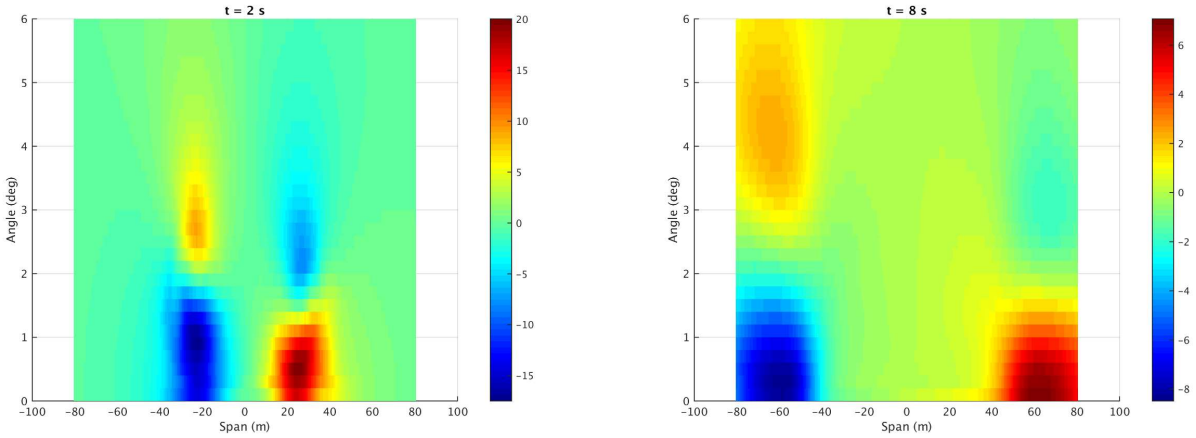
t = 2 s
Angle (deg)
Span (m)

t = 8 s
Angle (deg)
Span (m)

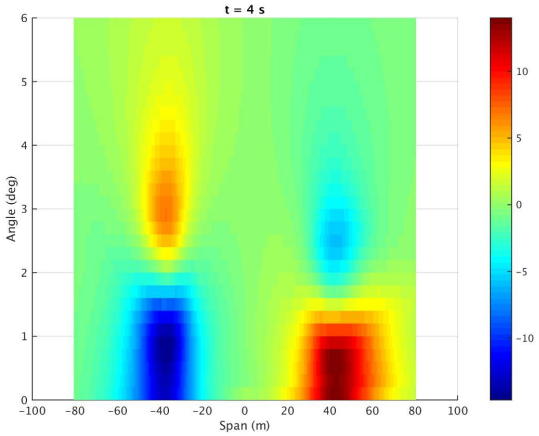
t = 4 s
Angle (deg)
Span (m)

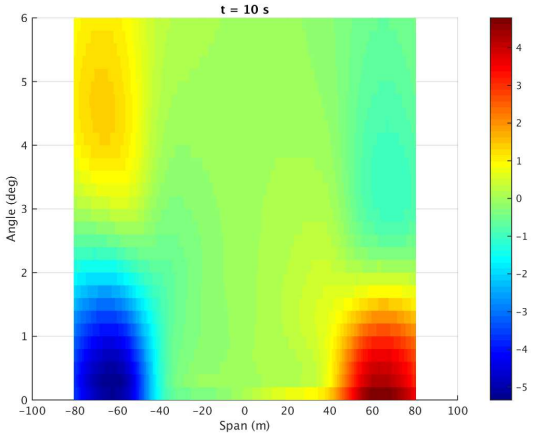
t = 10 s
Angle (deg)
Span (m)

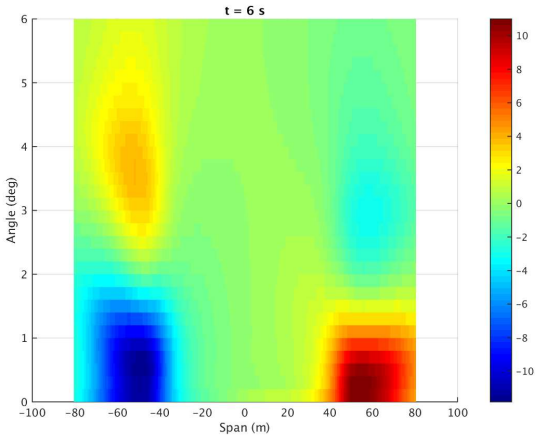
t = 6 s
Angle (deg)
Span (m)

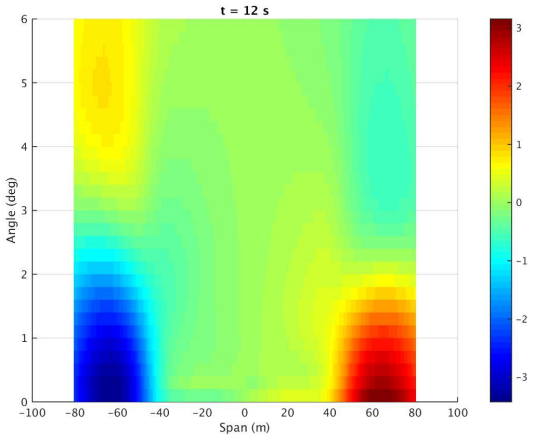
t = 12 s
Angle (deg)
Span (m)

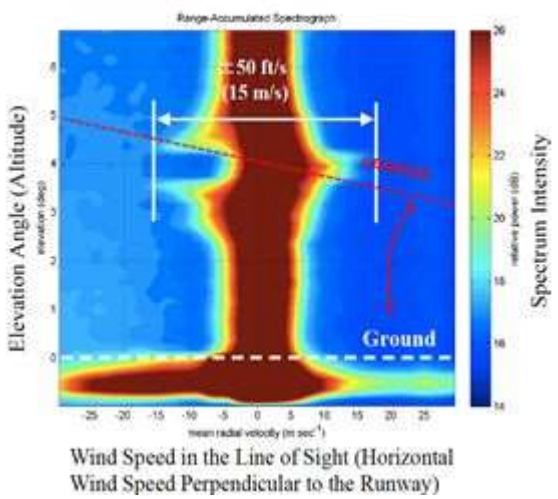

Fig. 22 CFD and LIDAR data showing the change of velocity due to the passage of the helicopter wake (UoG).

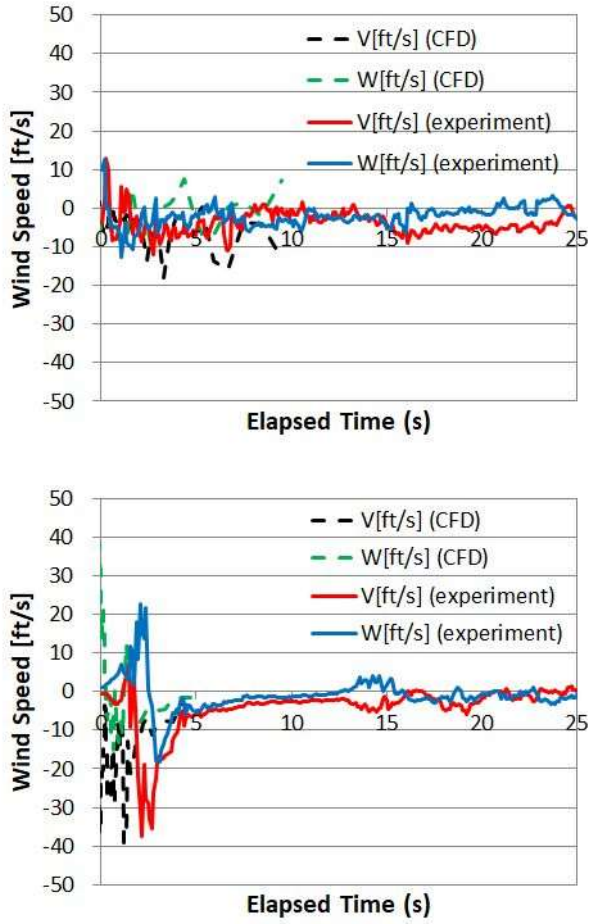

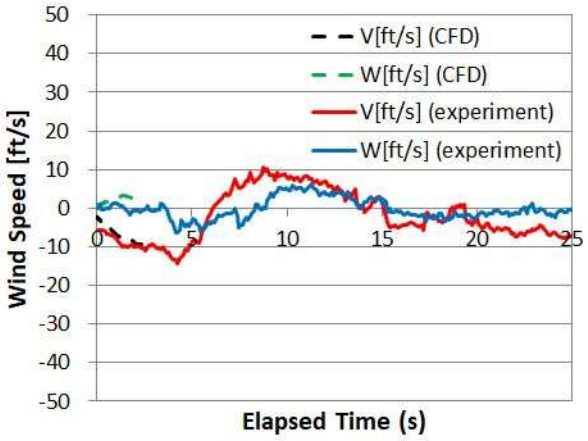

Fig. 23. Time histories of wind speed in CFD at position of ultrasonic anemometer #1 (JAXA).

5. CONCLUSIONS

In this study, the CFD codes of UoG and JAXA were compared for helicopter wakes in ground effect. Especially, steady computations were carried out for the case where the rotor is located 30 ft above the ground, at freestream velocities of 10, 20 and 40kts. CFD results were compared in terms of wake structure, vorticity distribution and vertical velocity. In addition, direct comparison with the experimental data such as LIDAR and ultrasonic anemometer data is also attempted. Through comparing numerical results of each party and flight experimental data, it is found that the CFD codes show qualitatively the same results each other and they are also close to the experiment. Considering the reported accidents in UK and Japan, wake modelling around a helicopter and far backward is expected to become useful in establishing guidelines for helicopter operations. To this end, further work is planned to model the velocity field variations with taxiing speed and altitude and results with CFD are to be reported in future papers.

REFERENCES

[1] Okuno, Y., and Matayoshi, N. Effects of Large Airplanes' Wake Turbulence on Small Aircraft, JAXA-RR-07-029, 2008 (In Japanese).

[2] CAA, Aircraft accident report 1/93. Technical report, Civil Aviation Authority, 1993.

[3] The Sankei Shimbun & SANKEI DIGITAL, 2016, http://www.sankei.com/affairs/news/160807/afr1608070019-n1.html

[4] Teager, S. A., Biehl, K. J., Garodz, L. J., Tymczyszym, J. J., and Burnham, D. C. Flight Test Investigation of Rotorcraft Wake Vortices in Forward

Flight, DOT/FAA/CT-94/117, 1996.

[5] Wang, Y., White, M., Barakos, G. N., Tormey, P., and Pantazopoulou, P. Simulation of a Light Aircraft Encountering a Helicopter Wake, Journal of Aircraft, Vol. 52, No. 2, 2015, pp. 510-523.

[6] Tanabe, Y., Saito, S., and Sugawara, H. Evaluation of Rotor Noise Reduction by Active Devices Using a CFD/CSD Coupling Analysis Tool Chain, 1st Asian Australian Rotorcraft Forum and Exhibition 2012 Proceedings, Busan, Korea, 2012.

[7] Tanabe, Y., Saito, S., Ooyama, N., and Hiraoka, K. Investigation of the Downwash Induced by Rotary Wings in Ground Effect, International Journal of Aeronautical and Space Sciences, Vol. 10, No., 1, 2009, pp. 20-29.

[8] Sugiura, M., Tanabe, Y., Sugawara, H., Matayoshi, N., and Ishii, H. Numerical Simulations and Measurements of the Helicopter Wake in Ground Effect, Journal of Aircraft, Vol. 54, No. 1, pp. 209-219, 2017.

[9] A. Humpert, Design of the new EUROCOPTER Medium Twin Helicopter EC145, 59th American Helicopter Society Annual Forum, Phoenix, Arizona, USA, 2003.

[10] Wang, Y., White, M., and Barakos, G.N. (2017) Wind-turbine wake encounter by light aircraft. Journal of Aircraft, 54(1), pp. 367-370.